Sensors and Actuators B 255 (2018) 1276–1284

Contents lists available at ScienceDirect

Sensors and Actuators B: Chemical

journal homepage: www.elsevier.com/locate/snb

Computational investigation of label free detection of biomolecules based on armchair graphene nanoribbon

S. Bagherzadeh-Nobari [a], R. Kalantarinejad [b,*], S.M. Elahi [a], S. Sanvito [c]

[a] Plasma Physics Research Center, Science and Research Branch, Islamic Azad University, Tehran, Iran
[b] Aerospace Research Institute, Ministry of Science, Research and Technology, Tehran, Iran
[c] School of Physics and CRANN Institute, Trinity College, Dublin 2, Ireland

ARTICLE INFO

Article history:
Received 12 April 2017
Received in revised form 11 July 2017
Accepted 12 August 2017
Available online 24 August 2017

Keywords:
Graphene nanoribbon
Biosensor
Amino acid
Quantum transport

ABSTRACT

We propose here an amino acid nanosensor based on a single armchair graphene nanoribbon (AGNR) connected to two gold electrodes. Using the non-equilibrium Green's function method for quantum transport together with density functional theory, we compute the electrical properties of the sensor before and after the adsorption of different amino acids on the AGNR. Our results show that there is a significant shift of the projected density of states and of the transmission function, *T*, upon adsorption with a distinct response depending on the specific amino acid. These results suggest that AGNRs may be employed as materials of choice in bio-sensorics.

1. Introduction

In areas such as biology, life science, chemistry and environmental sciences, a great deal of importance is given to ones' ability of detecting and measuring biomolecules with high sensitivity and accuracy [1–7]. One of the most important biomolecules in these areas are proteins. As an example since disease-pertubated proteins differ from their normal counterpart, detection and quantification of them will enable a predictive and preventive medicine that will lead to personalized medicine. Should this be possible in practice, we expect efficient protein sensors to contribute to the improvement of medicine and medical treatments. Amino acids are the building blocks of proteins. Furthermore detection of amino acids will help us in determining the nature of full proteins [8].

One and two dimensional nanostructures such as nanotubes, nanowireş graphene, silicene and hybrid sheets can form excellent technological platforms for single molecule recognition, because of the extreme sensitivity of the electron transport properties in extremely confined materials to external perturbations [9–19]. Recently biosensors based on field-effect-transistor (FET) architectures have attracted considerable attention, since the detection that they offer is rapiḍ inexpensive and label-free. In a FET biosensor, the physical gate active in logic transistors is removed and biomolecules instead produce the gating (electrostatic) effect. Such an effect is transduced into a readable signal in the form of one or many changes in the electrical characteristics of the FET, such as the drain-source current or the channel conductance. Among the various materials considered, nanostructured carbon nanotubes and Si nanowires appear to be the most attractive to the sensors community due to their size compatibility and capability to provide high sensitivity [20–24]. However, the fabrication of such devices often presents major challenges such as reproducibility and integrability with conventional architectures [25,26], thus it hampers their use in practice. In contrast, silicene and graphene-based structures are extremely promising, as they both provide excellent electrostatics due to their atomically thin nature and possess a planar geometry, which can be used in large-scale integrated device processing and fabrication.

There are some theoretical studies that investigated the capability of these materials as gas sensor or biosensor. Amorim et al., [14] showed that the adsorption of each nucleobase on the silicene sheet causes significant and distinct changes in the transmission at zero bias at specific energies. So silicene can be used as biosensor for DNA analysis. In another work, Prasongkit et al., [15] proposed a gas sensor based on silicene and showed that doping of silicene can enhance the sensitivity of the device and all of the four gas molecules (NO, NO_2, NH_3 and CO) can be distinguished.

Recently, Rodríguez et al., [16,17] theoretically modeled a two terminal device based on graphene and investigated the effect of

* Corresponding author.
E-mail addresses: kalantari@ari.ac.ir, rezakalantarinezhad@gmail.com (R. Kalantarinejad).

http://dx.doi.org/10.1016/j.snb.2017.08.113
0925-4005/

adsorption of amino acids on the electrical properties of graphene. Due to interaction between amino acids and graphene charge transfers from graphene to amino acid and current changes significantly. They showed that the device detects amino acids with high selectivity and sensitivity at specific bias voltages. The result shows that their sensor can be used as amino acid sequencer in proteins.

Unlike graphene, graphene nanoribbons may display an electronic band gap making them more sensitive to external perturbations than their bulk counterpart. Several groups worldwide have made progress towards the experimental demonstration of graphene-nanoribbon-based sensors [27–29]. Furthermore a few theoretical investigations prove the feasibility of such concept. For instance, Hossain et al., theoretically proposed a sensitive neurobiosensor based on a graphene nanoribbon for detection of glycine amino acid [19]. They showed that in the presence of glycine current increases significantly in two terminal device based on the graphene nanoribbon with nitrogen vacancy. The presence of the nitrogen vacancy in the graphene nanoribbon decreases current significantly at specific bias voltages. So their sensor can be used in proximity of living neuron cells due to reduction of power consumption.

However, often in the theoretical researches the external electrodes are not explicitly considered, i.e. the electrodes connecting the sensing nanoribbon are nanoribbons themselves [16,17,19,30–32]. In this paper, we aim to go beyond such a simplification and study the effects of amino acid adsorption on the conductance of single-layer armchair graphene nanoribbon in a simple two-probe configuration with Au electrodes.

In line with the conventional notation [33] an AGNR (a zigzag GNR ZGNR) is uniquely defined by the number, n, of dimer lines (zigzag chains) along the ribbon width. It has been shown in previous studies that all AGNRs are semiconductor while ZGNRs are metallic [33,34]. The energy gap of AGNRs decreases as a function of the ribbon width. In particular, the amplitude of the energy gap is different depending on whether $n = 3p$, $n = 3p + 1$ and $n = 3p + 2$ (p is integer). For $n = 3p + 1$ the energy gap is large, while the AGNRs with $n = 3p + 2$ bear the smallest gap [35]. In this work, we focus on semiconducting AGNRs with the largest possible energy gap and look at the $n = 34$ case. In fact, an external perturbation, like the one provided by a biomolecule, is expected to have a much smaller effect on the electronic properties of a metallic GNR than on semiconducting type.

Amino acids are chosen as the target molecules to be sensed. Understanding their interaction with GNRs will help us in understanding how full proteins, which are at present too complex to be simulated by the state-of-the-art *ab-initio* techniques used here, interact with GNRs. Molecular dynamics (MD) simulations are used to determine the relative coordinates of the GNR and the adsorbed biomolecule, and also to investigate the effects of hydrophobic interactions and van der Waals (VDW) forces on the adsorption of amino acids by the graphene nanoribbon. The coordinates cannot be calculated simply by system relaxation from density functional theory (DFT) simulations. The reason is that, although now DFT implements good approximations for the van der Waals forces, the system size investigated here makes it prohibitively expensive. At the same time van der Waals forces cannot be neglected since they play an important role in the interaction between the GNR and the amino acids. In addition, computational costs also prevent us from including explicitly water molecules in the simulations. This means that the results presented here are strictly applicable to the ultra-dry limit. Finally, the resulting geometries optimized by MD are used in DFT combined with the non-equilibrium Green's function method for quantum transport (DFT + NEGF) [36], which allow us to extract the transport properties of the junction. In our calculations we use the local density approximation (LDA) throughout [37].

2. Simulation details and method

In order to investigate the sensing ability of the proposed sensor, the transport properties of the AGNR sandwiched between gold electrodes before and after the adsorption of each amino acid are computed by using the ab initio electronic transport code SMEAGOL [38–40]. SMEAGOL implements the NEGF method within DFT. The system is divided into three regions, the left and right electrodes that, in our case are semi-infinite gold crystals oriented along the (111) direction, and the device region containing a 34-armchair graphene nanoribbon with a length of approximately 100 Å and a portion of the semi-infinite gold electrodes (five Au layers) at each side. The distance between the AGNR and the Au layers was set to 2 Å. We place each of the amino acids above the plane of the AGNR at a minimum initial distance of 1 Å, as shown in Fig. 1(b) and (d). We consider here dimers of the positively charged amino acid arginine (ARG) and the neutral non-aromatic amino acid isoleucine (ILE) to investigate the effect of different type of amino acids on the transport properties of the AGNR and show that to what extent the charge of the biomolecule contributes in the sensing mechanism. Each dimer has two residues, where the residue is the form taken by amino acids when they constitute a chain of peptides, or comprise parts of proteins [8].

Subsequently, we need to find the equilibrium distance between the amino acids and the AGNR. NAMD [41] molecular dynamics code is used to perform this task. In NAMD, the CHARMM force field [42] and TIP3P [43] water molecules were used. Carbon atoms of the GNR had been modeled as spot free of charge using the CHARMM parameters for sp^2 carbon. The device region was optimized, excluding the gold layers, in a water box through the minimization procedure of the NAMD package that functions as per conjugate gradient method [41]. Three unit cells of the AGNR at the left and right-hand side were fixed during the minimization in order to avoid a mismatch between the electrodes and the AGNR. Counter ions were included with the charged amino acid to neutralize the net charge (chlorine ions with arginine). By performing the atomic relaxation, a stable point for the system energy was reached. After minimization, the minimum distance between each dimer and the graphene nanoribbon was calculated to be 2.612 Å and 2.54 Å for ILE and ARG, respectively. The optimized geometries are shown in Fig. 1(c) and (e). The newly optimized atomic coordinates were then used for the transport calculations (water molecules and counter ions were removed at this point), where no more geometry optimization was carried out.

Here, the electron transport properties were extracted by using the DFT + NEGF code SMEAGOL, which employs the SIESTA code [44] as DFT platform. SMEAGOL uses DFT to build the Hamiltonian of the system, $H(n)$, as well as the overlap matrix, S. If α and β label the SIESTA basis set, which is made of multiple-zeta numerical atomic orbitals, ϕ^{α}, then $H(n)$ and S write

$$H_{IJ}^{\alpha\beta} = < \phi^{\alpha} | H(n) | \phi^{\beta} > \quad (1)$$

$$S_{IJ}^{\alpha\beta} = < \phi^{\alpha} | \phi^{\beta} > \quad (2)$$

where n is the electron density. Here, I and J are partition indexes and take values L, R or D to represent the left-hand and right-hand side electrode and the device region, respectively. The core quantity of the NEGF method is the retarded Green's function of the device region, which reads [39]

$$G_{\mathrm{D}}^{\mathrm{R}}(E) = \epsilon^{+} S_{DD} - H_{DD} - \Sigma_{\mathrm{L}}^{\mathrm{R}}(E) - \Sigma_{\mathrm{R}}^{\mathrm{R}}(E) \quad (3)$$

In the above equation $\Sigma_{\mathrm{L,R}}^{\mathrm{R}}(E)$ are the retarded self-energies of each electrode. These can be directly calculated as

$$\Sigma_{\mathrm{I}}^{\mathrm{R}}(E) = (\epsilon^{+} S_{DI} - H_{DI}) G_{\mathrm{II}}^{\mathrm{R}}(E) (\epsilon^{+} S_{ID} - H_{ID}) \quad (4)$$

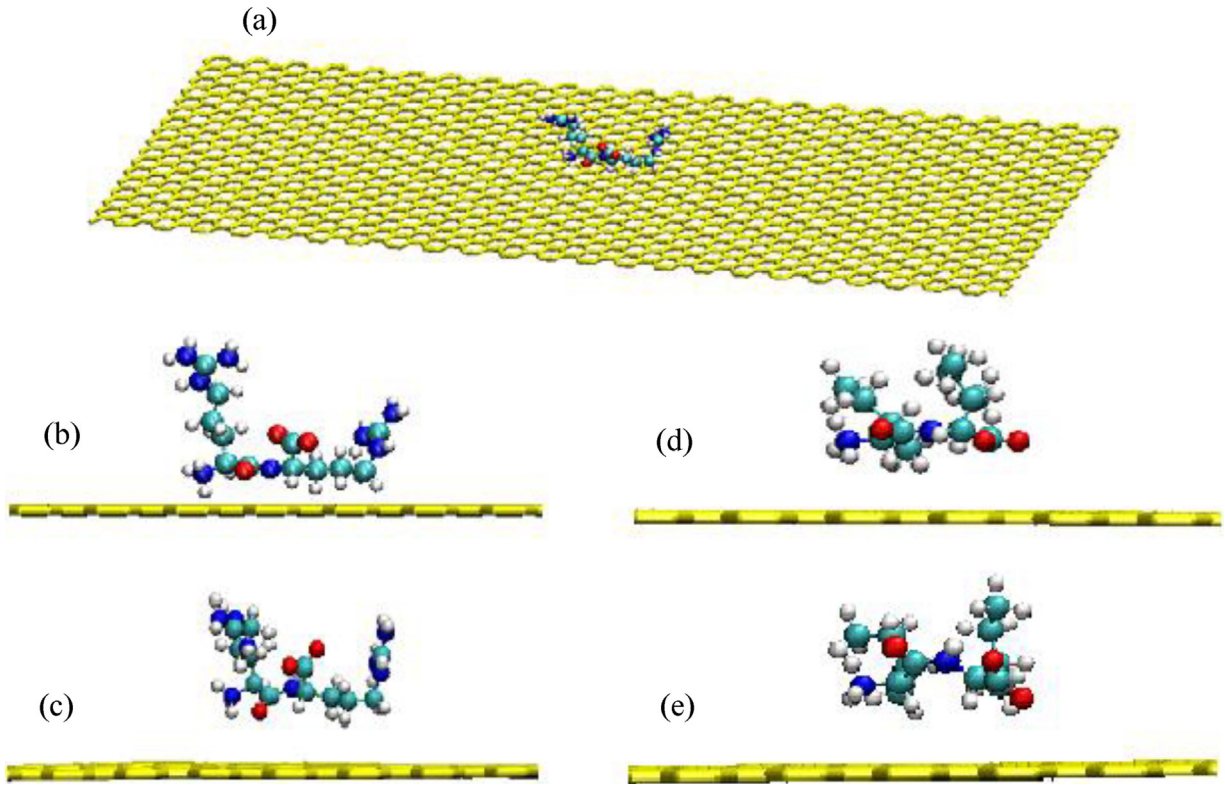

Fig. 1. The geometry of the different device structures investigated. Panel (a) shows general schematic view of initial configuration of ARG on the AGNR. Panels (b) and (c) show side view of ARG adsorbed on the AGNR, respectively before (b) and after (c) structural relaxation; panels (d) and (e) the same for ILE. Color code: light blue = C, dark blue = N, red = O, white = H. C atoms in the AGNR are shown in yellow.

with $\varepsilon^{+} = \lim_{\delta \to 0+} E + \mathrm{i}\delta$, E being the energy, $G_{\mathrm{II}}^{\mathrm{R}}$ represents the electrodes' retarded surface Green's function [39]. Despite the fact that Eq. (4) in principle involves multiplication of infinite matrices, a restricted form of $\Sigma_{\mathrm{L,R}}^{\mathrm{R}}(E)$ exists. This involves unit cells information only along with the coupling of the electrodes' surfaces to the device region [45,46]. The electron density is $n(\vec{r}) = < \vec{r}|D|\vec{r}$ where D represents the density matrix. This can be evaluated for our open boundary conditions problem from the lesser Green's function, $G_{\mathrm{D}}^{<}$ as [39]

$$D = \frac{1}{2\pi \mathrm{i}} \int G_{\mathrm{D}}^{<}(E)\mathrm{d}E \tag{5}$$

The lesser Green's function at equilibrium, i.e. in the zero-bias limit investigated here, is written as $G_{\mathrm{D}}^{<}(E) = -2\mathrm{i}\mathrm{Im}[G_{\mathrm{D}}^{\mathrm{R}}(E)]f(E-\mu)$ [38], with f being the Fermi function at the electronic temperature T. The set of Eq. (1)–(5) constructs a self-consistent procedure that is solved in an iterative manner to yield $G_{\mathrm{D}}^{\mathrm{R}}$, i.e. the electronic structure of the device region in equilibrium with the electrodes. The outcome of such iterative calculation can be directly used for computing the system zero-bias conductance, G. This is obtained through the Fisher–Lee relation as

$$G = \frac{2\mathrm{e}^2}{h}\mathrm{Tr}[\Gamma_{\mathrm{L}} G_{\mathrm{D}}^{\mathrm{R}*} \Gamma_{\mathrm{R}} G_{\mathrm{D}}^{\mathrm{R}}] \tag{6}$$

where

$$\Gamma_{\mathrm{L,R}}(E) = \mathrm{i}[\Sigma_{\mathrm{L,R}}^{\mathrm{R}}(E) - \Sigma_{\mathrm{L,R}}^{\mathrm{R}*}(E)] \tag{7}$$

Note that Eq. (6) calculates the conductance as the product of the quantum of conductance, $G_{0} = 2\mathrm{e}^2/\mathrm{h}$, with the energy dependent transmission coefficient, evaluated at the Fermi energy of electrodes, i.e. for $E = E_{\mathrm{F}}$. In order to save computational time, we have used a single zeta basis sets for the AGNR atoms. This is justified by the fact that only the states around E_{F} are crucial to the transport properties [47]. Concerning gold atoms, a well-tested strategy has been conducted [48] taking into account solely the 6*s* shell as valence and leaving the 5*d* orbitals in the core. This is a good approximation for moderate bias, since the 5*d* orbitals contribute little to the Au Fermi surface. Only a single zeta polarized basis set [49] is used for all the atoms in the amino acids, while the only exceptions are H and C, for which a single zeta basis is utilized to cut down on the computational time. We use the LDA in the Ceperley–Alder [50] parameterization to describe the exchange–correlation energy. We have chosen the convergence tolerance of the density matrix to be 10^{-4}, while the real-space grid has a plane-wave cut-off corresponding to 200 Ry. The electronic structure of the electrodes is calculated with a uniformly spaced k-point grid of $1 \times 1 \times 30$, and the unit cell contains 315 atoms. All transport calculations are done at zero-bias voltage. We have used a supercell of $50.26 \times 23.65 \times 125.88$ Å. The supercell size is chosen to avoid any image-cell interaction. We have used periodic boundary conditions in the direction orthogonal to the transport direction.

3. Results and discussions

In this work, we aim to study the sensing ability of the device. As such, we have investigated and compared the electrical properties of the AGNR before and after the adsorption of each amino acid. First we have computed the optimized structure of the sensor via MD simulations. Then the projected density of states (PDOS) over the AGNR and the transmission coefficient at zero bias are calculated. These are presented in Fig. 2, where we set the energy zero to the Au Fermi energy. Since the spectral range contributing to the conduction is $\pm 8k_{\mathrm{B}}T$ around the Fermi level ($k_{\mathrm{B}}T$ is the thermal energy with k_{B} the Boltzmann constant), which corresponds to ±0.2 eV in our case (T is room temperature), we have plotted the PDOS and T in the range ±0.3 eV. At this juncture and moving for-

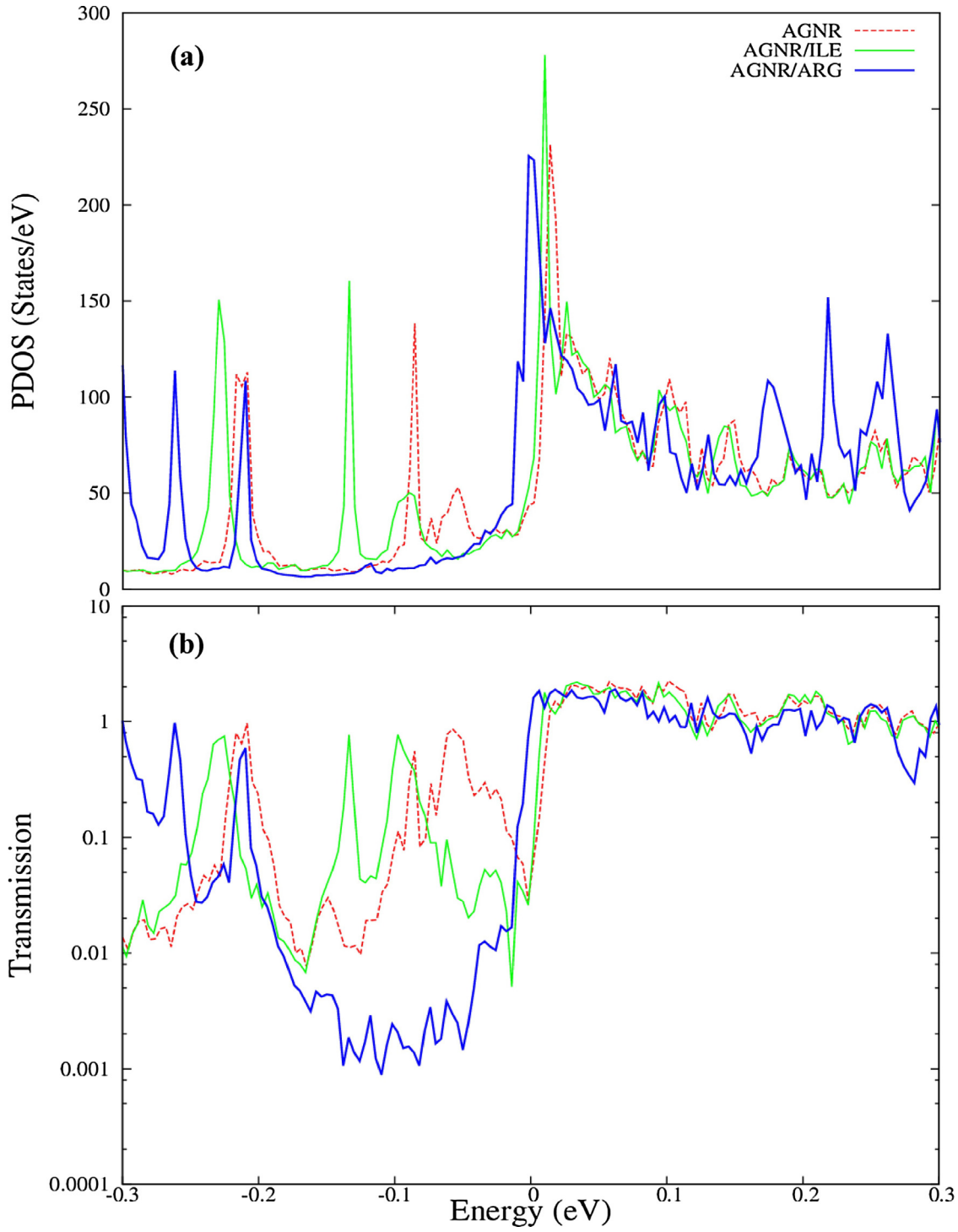

Fig. 2. Electronic structure and transport properties of the junctions investigated. (a) PDOS over the AGNR and (b) transmission coefficient, $T(E)$, as a function of energy. Here, $T(E)$ is plotted in logarithmic scale. The various curves represent the case of pristine AGNR (dashed red line), AGNR with adsorbed ILE (thin solid green line) and AGNR with adsorbed ARG (thick solid blue line). (For interpretation of the references to colour in this figure legend, the reader is referred to the web version of this article.)

ward we shall analyze the results by looking at the case of a pristine AGNR.

In Fig. 2(a) (dashed red curve) we present the PDOS of the AGNR sandwiched between the two Au electrodes and observe that the electrode Fermi level just cuts at the bottom of the conduction band of the AGNR. In fact we find that the PDOS sharply increases for positive energy, while it is composed of a number of localized states emerging from a low-PDOS background for negative ones. Such PDOS structure reflects into the behaviour of the transmission coefficient as a function of energy shown in Fig. 2(b). Here we can see that $T(E)$ sharply increases from zero to about 1.5 at the onset of the AGNR conduction band placed roughly at $E = E_F$. In the gap region we can identify two sets of peaks positioned in the energy window going from 0 eV to −0.3 eV. The first is between −0.05 eV and −0.1 eV and is formed by a doublet with a sharp peak at −0.1 eV and a broader shoulder at −0.05 eV. The second is also a doublet formed by two closely-spaced sharp peaks at around −0.2 eV. Note that the presence of a finite DOS even in the AGNR gap is associated to the

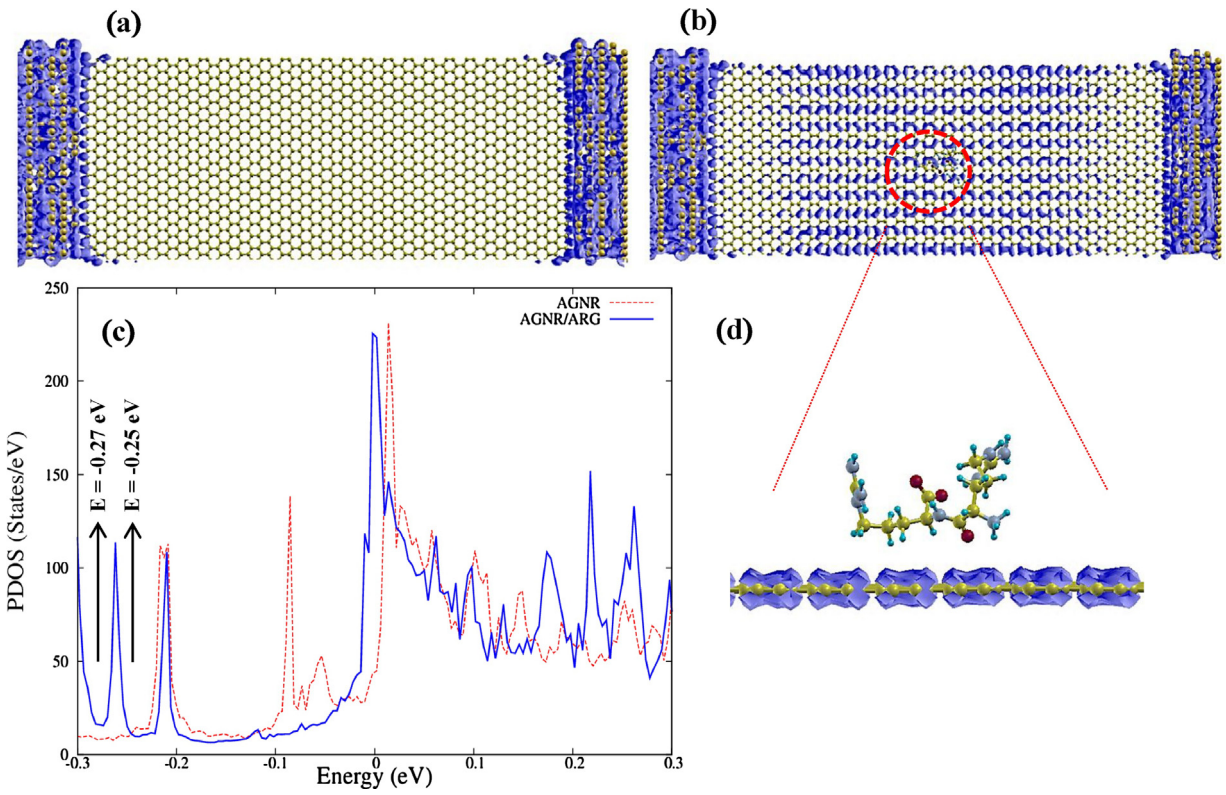

Fig. 3. The top panels show the local density of state iso-surfaces of the junction (in blue) (left) before and (right) after the adsorption of ARG on the AGNR. The iso-surfaces are taken for the energy range $-0.27 < E < -0.25$ eV. The isovalue is 0.00005 e/Å^3. Bottom-left figure shows the PDOS of the bare AGNR (dashed red line) and of the AGNR with ARG adsorbed (thick solid blue line). Arrows defines the energy range corresponding to the LDOS. Bottom-right figure shows side view of the LDOS of ARG adsorbed on the AGNR. (For interpretation of the references to colour in this figure legend, the reader is referred to the web version of this article.)

evanescent states, surface states, originating from the gold contacts [51,52]. According to Fig. 2, we can observe that two factors contribute in the conductance of the AGNR: (i) the conductance due to states in the conduction band near the Fermi energy (because semiconductor is *n*-type) and (ii) mid-gap tunnelling conductance due to mid-gap states.

The adsorption of the amino acids changes both the PDOS and the transmission function of the junction. When ILE is attached to the AGNR there is a general shift of the entire PDOS and of the $T(E)$ profile to lower energies (see thin solid green lines in Fig. 2). Such a shift is moderate at the Fermi level (the sharp onset of the conductance at $E \sim E_F$ remains almost at the same energy) but it is appreciable in the band-gap region. In particular the doublet originally placed at around −0.1 eV is now almost rigidly shifted down by about 0.05 eV, while originally at −0.2 eV it is pushed down in energy by about 0.025 eV. Such energy downshift in the band-gap spectral region is reflected into a general deformation of the transmission function $T(E)$ associated to the peaks in the PDOS, although the double structure remains well visible in Fig. 2(b).

Finally, we turn our attention to the case of ARG adsorbed on the AGNR. After adsorption of ARG new states appear in the conduction band edge and also the conduction band shifts considerably to lower energies which now the fermi energy cuts through the bottom of the AGNR conduction band and yields a large transmission coefficient (large zero-bias conductance). In the gap region the peak structure appears quite different from that of the pristine AGNR and that modified by ILE adsorption, with no peaks around the Fermi level (the features at −0.1 eV are no longer visible either in the PDOS or in the transmission coefficient). Instead two singlets are clearly visible at −0.2 eV and −0.25 eV. The new states can be caused by the interaction of ARG with AGNR. In this case, in contrast with the case of the pristine AGNR and the AGNR modified with ILE only states in the conduction band near the Fermi level contribute in the conduction because the localized states in energy range around −0.1 eV disappear after adsorption of ARG.

In order to demonstrate this conjecture we have calculated the real space local density of states (LDOS) of the AGNR before and after the adsorption of ARG in the energy range $-0.27 < E < -0.25$ eV, i.e. where the new peaks are positioned (see Fig. 3). From the figure it is quite clear that in the case of the pristine AGNR, the only DOS in such spectral region originates from the Au electrodes, as expected from the fact that this energy window is well within the AGNR bandgap. In contrast when ARG is adsorbed there is now a significant contribution from both the ARG molecule itself and the surrounding region on the ribbon. This clearly indicates that the new peak is related to a hybrid ARG/AGNR state.

Furthermore, we have investigated why the adsorption of ARG suppresses the PDOS peaks observed in the gap region for the pristine case. In Fig. 4 we present the calculated LDOS before and after ARG adsorption in the energy range around −0.1 eV, i.e. in the energy window corresponding to the first double peak structure for the pristine AGNR. We find that such peak structure is associated with LDOS concentrated at the ribbon edges facing the Au electrodes and at the ribbon center. This effectively corresponds to a ribbon quantum-well state with maximum amplitude at the ribbon center, namely to a node-less wave function. When the ARG amino acid is adsorbed in the middle of the ribbon its interaction with such quantum-well state is maximized and the state is pushed at higher energies, where it merges with the continuum of states provided by the ribbon conduction band.

Our results and sensing mechanism can be due to different reasons such as electrostatic gating of the channel and/or charge transfer between the channel and the target molecule to be sensed. There are several theoretical studies that investigated the sensing

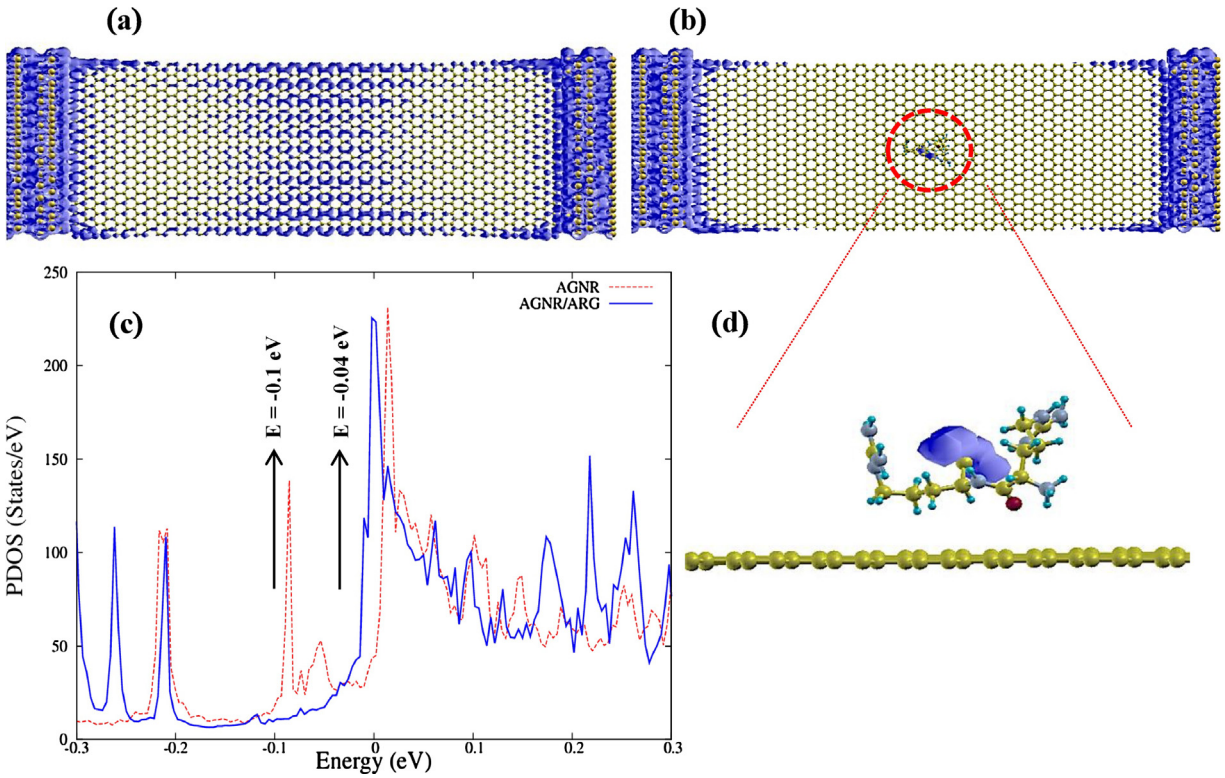

Fig. 4. The top panels show the local density of state isosurfaces of the junction (in blue) (left) before and (right) after the adsorption of ARG on the AGNR. The isosurfaces are taken for the energy range $-0.1 < E < -0.04$ eV. The isovalue is 0.0001 e/Å^3. Bottom-left figure shows the PDOS of the bare AGNR (dashed red line) and of the AGNR with ARG adsorbed (thick solid blue line). Arrows defines the energy range corresponding to the LDOS. Bottom-right figure shows side view of the LDOS of ARG adsorbed on the AGNR. (For interpretation of the references to colour in this figure legend, the reader is referred to the web version of this article.)

Table 1
Charge transfer from each dimer to the AGNR and dipole of ILE and ARG.

Dimer	ILE	ARG
Dipole of dimer (D)	16.02	5.768
Charge transfer from dimer to the AGNR (|e|)	0.744	2.219

mechanism of FET biosensors. For instance, de Souza et al., proposed a novel nanopore architecture in a hybrid sheet (graphene nanoroad embedded in hexagonal boron nitride sheet) that can be used to distinguish four different nucleotides electrically [18]. In this system, local current that is concentrated in the gaphene nanorod is sensitive to the dipole of the molecule in vicinity of it. So each nucleotide with distinct dipole acts as an electrostatic gate (each nucleotide redistributes charge distinctly in the graphene nanorod) and modulates the current. Rodríguez et al., [16,17] showed the sensing mechanism in their amino acid sensor is due to existence of longitudinal and transverse dipoles through charge transfer from graphene to amino acids that changes the electrical properties of the device. Feliciano et al., [53] demonstrated that negatively charged nucleotides in a graphene nanopore act as local gate and shift the conductance to higher energies. Amount of charge and as a result electrostatic gate is changed due to charge transfer between each base and the graphene nanopore.

In order to rationalize our results and determine sensing mechanism in our device, we have computed the dimers dipole and the charge transfer between the AGNR and the dimers (see Table 1). The Mülliken population method was adopted to analyze the charge distribution, meaning that differences between the various Mülliken populations depicts the charge transfer. According to Table 1, the AGNR acts as a charge acceptor in all cases, thus n-doping happens simply because of the presence of the electrodes. Furthermore, upon amino acid adsorption additional electronic charge is transferred to the ribbon. This is significantly more pronounced in the case of ARG, which can transfer approximately 2 electrons to the ribbon, while only about 0.7 electrons are transferred from ILE. Such a significant difference in electron transfer between the two amino acids explains the different positions of the Au Fermi level with respect to the ribbon conduction band.

Further insights can also be obtained from a charge density difference plot, which is presented in Fig. 5 for the case of ARG adsorption. This is defined as

$$n_{diff}(\vec{r}) = n_{AGNR-dimer}(\vec{r}) - n_{AGNR}(\vec{r}) - n_{dimer}(\vec{r}) \quad (8)$$

where $n_{AGNR}(\vec{r})$ and $n_{dimer}(\vec{r})$ are the charge densities of the complex dimer-AGNR of the pristine AGNR and of the dimer, respectively. The figure confirms that there is a significant transfer of charge from the ARG dimer (blue surface) to the AGNR (red surface). The charge transfer creates a vertical dipole in the center of the ribbon. Also a horizontal charge polarization over the graphene nearer to the electrodes forms a local longitudinal dipole [17]. Interestingly, the electrons donated by the amino acid mostly remain localized in the central region of the ribbon, where they electrostatically interact with the positively charged molecule, and at the ribbon edges with the Au electrodes. Overall, it seems that the molecule absorption drastically increases the AGNR carrier density. It is due to the charge transfer and the electrostatic gating. The electrostatic gating is dominated in the case of ILE due to the dipole of ILE (because in this case the charge transfer is negligible). But in the case of ARG both of them contribute in doping. In this case direct doping happened due to significant charge transfer which causes appearing new states in the conduction band edge. The AGNR is doped indirectly by electrostatic gating. There is a shift to lower energy in PDOS due to three reasons, the electrical dipole, the charge of

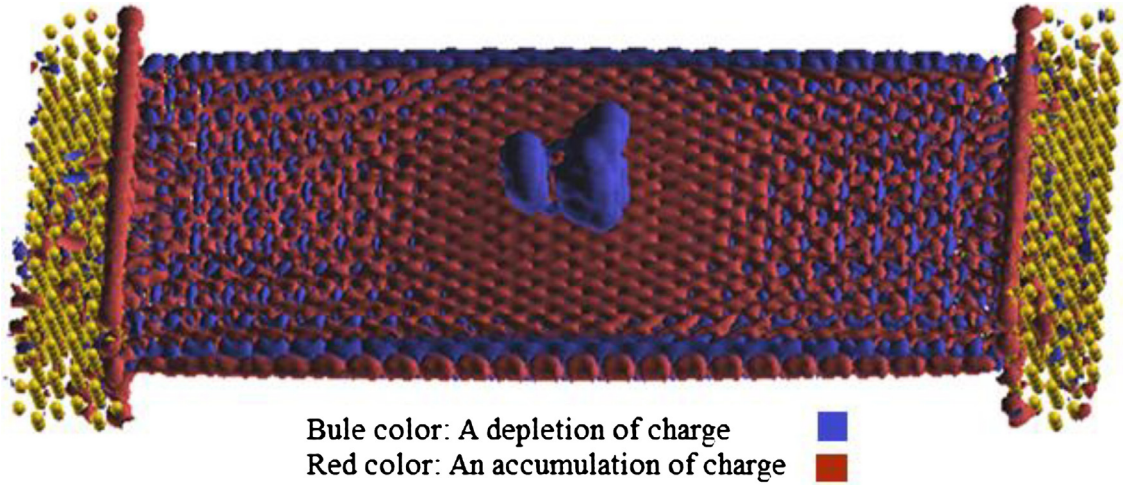

Fig. 5. Charge density difference for the ARG dimer adsorbed on the AGNR surface. The charge transfer from blue to red regions. The isovalue is 0.000001 e/Å^3. (For interpretation of the references to colour in this figure legend, the reader is referred to the web version of this article.)

Table 2
Summary of the calculated linear response conductance.

Sensor	Pristine AGNR	AGNR/ILE	AGNR/ARG
Conductance (G/G_0)	0.0453	0.0546	1.1764

molecule and the extra charge of the molecule. All of these charges act as a positive gate.

Finally, in Table 2 we present the zero-bias conductance of the AGNR before and after the adsorption of the dimers. For both ARG and ILE there is an increase in conductance upon absorption, which directly corresponds to the downshift in energy of the ribbon conduction band with respect to the electrodes Fermi level. Such an increase is only minor in the case of ILE, for which the shift is almost undetectable, but it is significant for ARG, since the charge transfer is sufficient to make the device completely metallic. As such, we conclude that our proposed sensor should be well capable of detecting the absorption of ARG by simply monitoring the zero-bias conductance. In contrast the detection of ILE will require collecting more information about the transmission coefficient as a function of energy, namely it will require a more detailed knowledge of the current-voltage characteristic and its derivatives.

The question that may arise is whether the sensing ability will survive in biological conditions (water and counter ions) or not? There are some theoretical studies [53,54] that investigated the effect of solvent on the transport properties of their systems. Rungger et al., [54] investigated the effect of water on the transport properties of polar and non-polar systems. They showed that water acts as electrostatic gate on polar molecule due to its time-averaged dipolar field resulting in the considerable shift of the transmission spectrum. But for non-polar system, time-averaged dipolar field of ware is zero and water has no electrostatic gating effect.

In another work, Feliciano et al., [53] applied a quantum-classical hybrid method to investigate the ability of graphene nanopore as DNA sequencer in solvent. They included the structural fluctuations of the system by MD simulation and for each snap-shot they considered the effect of counter ions, solvent and other nucleotides that is not in the pore as an external potential in kohn-sham equation for the quantum system that is composed of the graphene nanopore and one nucleotide in it. They showed that negative charge of each nucleotide in the nanopore acts as electrostatic gate and shifts the transmission spectrum. Due to the structural fluctuation of the system, charge fluctuations occur on each nucleotide that cause fluctuations in the conductance. They also showed that the charge is stabilized only when water and counter ions are considered. Although the charge of the molecule and charge transfer between graphene and nucleotides are changed in the presence of solvent, in general mechanism of sensing is not changed.

In general, we expect that environment affects the transport properties of the system that comprises polar and charged molecules. So this issue should be investigated in future studies. Due to computational limitations we are not able to include water and counter ions in our simulation. However, we are going to use the quantum-classical hybrid method that Feliciano et al., [53] has applied to investigate the effects of the environment on the transport properties of our system.

4. Conclusion

In this work we have studied the effects of amino acids adsorption on the electrical properties of an AGNR sandwiched between two gold electrodes at zero bias. A modification of the PDOS, and hence of the transmission, is obtained upon adsorption of two amino acids on the GNR surface. The change in PDOS and T is distinct for each amino acid. Overall, we have found that adsorption of ILE and ARG dimers increases the PDOS around E_F, resulting in enhanced linear response for conductance. This enhancement is different for ILE and ARG, and it is significantly more pronounced for ARG. Our electron transport results are rationalized in terms of charge transfer from the amino acid to the ribbon and dipole of the molecules, and suggest that AGNRs may be a promising materials platform for the fabrication of bio-molecular FET-like sensors.

References

[1] S.H. Lim, L. Feng, J.W. Kemling, C.J. Musto, K.S. Suslick, An optoelectronic nose for detection of toxic gases, Nat. Chem. 1 (2009) 562–567, http://dx.doi.org/10.1038/nchem.360.
[2] F. Bano, L. Fruk, B. Sanavio, M. Glettenberg, L. Casalis, C.M. Niemeyer, et al., Toward multiprotein nanoarrays using nanografting and DNA directed immobilization of proteins, Nano Lett. 9 (2009) 2614–2618, http://dx.doi.org/10.1021/nl9008869.
[3] M. Zwolak, M. Di Ventra, Colloquium. Physical approaches to DNA sequencing and detection, Rev. Mod. Phys. 80 (2008) 141–165, http://dx.doi.org/10.1103/RevModPhys.80.141.
[4] C.P. Fredlake, D.G. Hert, E.R. Mardis, A.E. Barron, What is the future of electrophoresis in large-scale genomic sequencing, Electrophoresis 27 (2006) 3689–3702, http://dx.doi.org/10.1002/elps.200600408.
[5] P. Jonkheijm, D. Weinrich, H. Schröder, C.M. Niemeyer, H. Waldmann, Chemical strategies for generating protein biochips, Angew. Chem. Int. Ed. 47 (2008) 9618–9647, http://dx.doi.org/10.1002/anie.200801711.

[6] F. Patolsky, G. Zheng, C.M. Lieber, Fabrication of silicon nanowire devices for ultrasensitive, label-free, real-time detection of biological and chemical species, Nat. Protoc. 1 (2006) 1711–1724, http://dx.doi.org/10.1038/nprot.2006.227.
[7] J.M. Vidic, J. Grosclaude, M.-A. Persuy, J. Aioun, R. Salessea, E. Pajot-Augy, Quantitative assessment of olfactory receptors activity in immobilized nanosomes: a novel concept for bioelectronic nose, Lab Chip. 6 (2006) 1026–1032, http://dx.doi.org/10.1039/b603189g.
[8] D. Whitford, Proteins: Structure and Function, John Wiley and Sons Ltd, Chichester, 2005.
[9] G. Zhang, P. Qi, X. Wang, Y. Lu, X. Li, R. Tu, et al., Selective etching of metallic carbon nanotubes by gas-phase reaction, Science 314 (2006) 974–977, http://dx.doi.org/10.1126/science.1133781.
[10] J.C. Meyer, A.K. Geim, M.I. Katsnelson, K.S. Novoselov, T.J. Booth, S. Roth, The structure of suspended graphene sheets, Nature 446 (2007) 60–63, http://dx.doi.org/10.1038/nature05545.
[11] E. Shapir, H. Cohen, A. Calzolari, C. Cavazzoni, D.A. Ryndyk, G. Cuniberti, et al., Electronic structure of single DNA molecules resolved by transverse scanning tunnelling spectroscopy, Nat. Mater. 7 (2008) 68–74, http://dx.doi.org/10.1038/nmat2060.
[12] N. Kang, A. Erbe, E. Scheer, Electrical characterization of DNA in mechanically controlled break-junctions, New J. Phys. 10 (2008) 023030, http://dx.doi.org/10.1088/1367-2630/10/2/023030.
[13] B. Song, M. Elstner, G. Cuniberti, Anomalous conductance response of DNA wires under stretching, Nano Lett. 8 (2008) 3217–3220, http://dx.doi.org/10.1021/nl801542g.
[14] R.G. Amorim, R.H. Scheicher, Silicene as a new potential DNA sequencing device, Nanotechnology 26 (2015) 154002, http://dx.doi.org/10.1088/0957-4484/26/15/154002.
[15] J. Prasongkit, R.G. Amorim, S. Chakraborty, R. Ahuja, R.H. Scheicher, V. Amornkitbamrung, Highly sensitive and selective gas detection based on silicene, J. Phys. Chem. C 119 (2015) 16934–16940, http://dx.doi.org/10.1021/acs.jpcc.5b03635.
[16] S.J. Rodríguez, L. Makinistian, E.A. Albanesi, Graphene for amino acid biosensing: theoretical study of the electronic transport, Appl. Surf. Sci. 419 (2017) 540–545, http://dx.doi.org/10.1016/j.apsusc.2017.05.031.
[17] S.J. Rodríguez, L. Makinistian, E. Albanesi, Computational study of transport properties of graphene upon adsorption of an amino acid: importance of including -NH_2 and-COOH groups, J. Comput. Electron. 16 (2017) 127–132, http://dx.doi.org/10.1007/s10825-016-0943-x.
[18] F.A. de Souza, R.G. Amorim, W.L. Scopel, R.H. Scheicher, Electrical detection of nucleotides via nanopores in a hybrid graphene/h-BN sheet, Nanoscale 9 (2017) 2207–2212, http://dx.doi.org/10.1039/C6NR07154F.
[19] F.M. Hossain, F. Al-Dirini, E. Skafidas, A graphene nanoribbon neuro-sensor for glycine detection and imaging, J. Appl. Phys. 115 (2014) 214303, http://dx.doi.org/10.1063/1.4880744.
[20] N. Gao, W. Zhou, X. Jiang, G. Hong, T. Fu, C.M. Lieber, General strategy for biodetection in high ionic strength solutions using transistor-based nanoelectronic sensors, Nano Lett. 15 (2015) 2143–2148, http://dx.doi.org/10.1021/acs.nanolett.5b00133.
[21] R. Kalantari-Nejad, M. Bahrami, H. Rafii-Tabar, I. Rungger, S. Sanvito, Computational modeling of a carbon nanotube-based DNA nanosensor, Nanotechnology 21 (2010) 445501, http://dx.doi.org/10.1088/0957-4484/21/44/445501.
[22] G.B. Abadir, K. Walus, D.L. Pulfrey, Bias-dependent amino-acid-induced conductance changes in short semi-metallic carbon nanotubes, Nanotechnology 21 (2010) 015202, http://dx.doi.org/10.1088/0957-4484/21/1/015202.
[23] G.B. Abadir, K. Walus, R.F.B. Turner, D.L. Pulfrey, Effect of Single-biomolecule Adsorption on the Electrical Properties of Short Carbon Nanotubes, Proceeding of the 8th IEEE Conference on Nanotechnology, Arlington TX, 2008, pp. 230–232, http://dx.doi.org/10.1166/jnn.2008.008.
[24] X. Chen, I. Rungger, C.D. Pemmaraju, U. Schwingenschlögl, S. Sanvito, First-principles study of high conductance DNA sequencing with carbon nanotube electrodes, Phys. Rev. B 85 (2012) 115436, http://dx.doi.org/10.1103/PhysRevB.85.115436.
[25] M.S. Makowski, A. Ivanisevic, Molecular analysis of blood with micro/nano scale field effect transistor biosensors, Small 7 (2011) 1863–1875, http://dx.doi.org/10.1002/smll.201100211.
[26] W. Yang, K.R. Ratinac, S.P. Ringer, P. Thordarson, J.J. Gooding, F. Braet, Carbon nanomaterials in biosensors: should you use nanotubes or graphene, Angew. Chem. Int. Ed. 49 (2010) 2114–2138, http://dx.doi.org/10.1002/anie.200903463.
[27] Z.J. Qi, J.A. Rodríguez-Manzo, A.R. Botello-Meíndez, S.J. Hong, E.A. Stach, Y.W. Park, et al., Correlating atomic structure and transport in suspended graphene nanoribbons, Nano Lett. 14 (2014) 4238–4244, http://dx.doi.org/10.1021/nl501872x.
[28] Z.J. Qi, C. Daniels, S.J. Hong, Y.W. Park, V. Meunier, M. Drndic, et al., Electronic transport of recrystallized freestanding graphene nanoribbons, ACS Nano 9 (2015) 3510–3520, http://dx.doi.org/10.1021/nn507452g.
[29] B. Song, G.F. Schneider, Q. Xu, G. Pandraud, C. Dekker, H. Zandbergen, Atomic-scale electron-beam sculpting of near-defect-free graphene nanostructures, Nano Lett. 11 (2011) 2247–2250, http://dx.doi.org/10.1021/nl200369r.
[30] R. Chowdhury, F. Scarpa, S. Adhikari, Molecular-scale bio-sensing using armchair graphene, J. Appl. Phys. 112 (2012) 014905, http://dx.doi.org/10.1063/1.4733689.
[31] E.-C. Lee, Effects of DNA nucleotide adsorption on the conductance of graphene nanoribbons from first principles, Phys. Rev. Lett. 100 (2012) 153117, http://dx.doi.org/10.1063/1.3703603.
[32] M. Berahman, M.H. Sheikhi, Hydrogen sulfide gas sensor based on decorated zigzag graphene nanoribbon with copper, Sens. Actuators B 219 (2015) 338–345, http://dx.doi.org/10.1016/j.snb.2015.04.114.
[33] K. Nakada, M. Fujita, G. Dresselhaus, M.S. Dresselhaus, Edge state in graphene ribbons: nanometer size effect and edge shape dependence, Phys. Rev. B. 54 (1996) 17954–17961, http://dx.doi.org/10.1103/PhysRevB.54.17954.
[34] Q. Yan, B. Huang, J. Yu, F. Zheng, J. Zang, J. Wu, et al., Intrinsic current-voltage characteristics of graphene nanoribbon transistors and effect of edge doping, Nano Lett. 7 (2007) 1469–1473, http://dx.doi.org/10.1021/nl070133j.
[35] Y. Son, M.L. Cohen, S.G. Louie, Energy gaps in graphene nanoribbons, Phys. Rev. Lett. 97 (2006) 216803, http://dx.doi.org/10.1103/PhysRevLett.97.216803.
[36] K. Stokbro, J. Taylor, M. Brandbyge, H. Guo, Ab-initio non-equilibrium Green's function formalism for calculating electron transport in molecular devices, in: G. Cunberti, G. Fagas, K. Richter (Eds.), Introducing Molecular Electronics (Lecture Notes in Physics), Springer, Heidelberg, 2005, pp. 117–151.
[37] J.P. Perdew, A. Zunger, Self-interaction correction to density-functional approximations for many-electron systems, Phys. Rev. B 23 (1981) 5048–5079, http://dx.doi.org/10.1103/PhysRevB.23.5048.
[38] I. Rungger, S. Sanvito, Algorithm for the construction of self-energies for electronic transport calculations based on singularity elimination and singular value decomposition, Phys. Rev. B. 78 (2008) 035407, http://dx.doi.org/10.1103/PhysRevB.78.035407.
[39] A.R. Rocha, V.M. García-suárez, S.W. Bailey, C.J. Lambert, J. Ferrer, S. Sanvito, Towards molecular spintronics, Nat. Mater. 4 (2005) 335–339, http://dx.doi.org/10.1038/nmat1349.
[40] A.R. Rocha, V.M. García-suárez, S.W. Bailey, C.J. Lambert, J. Ferrer, S. Sanvito, Spin and molecular electronics in atomically generated orbital landscapes, Phys. Rev. B. 73 (2006) 085414, http://dx.doi.org/10.1103/PhysRevB.73.085414.
[41] J.C. Phillips, R. Braun, W. Wang, J. Gumbart, E. Tajkhorshid, E. Villa, et al., Scalable molecular dynamics with NAMD, J. Comput. Chem. 26 (2005) 1781–1802, http://dx.doi.org/10.1002/jcc.20289.
[42] A.D. Mackerell, D. Bashford, M. Bellott, R.L. Dunbrack, J.D. Evanseck, M.J. Field, et al., All-atom empirical potential for molecular modeling and dynamics studies of proteins, J. Phys. Chem. B. 102 (1998) 3586–3616, http://dx.doi.org/10.1021/jp973084f.
[43] W.L. Jorgensen, J. Chandrasekhar, J.D. Madura, R.W. Impey, M.L. Klein, Comparison of simple potential functions for simulating liquid water, J. Chem. Phys. 79 (1983) 926–935, http://dx.doi.org/10.1063/1.445869.
[44] J.M. Soler, E. Artacho, J.D. Gale, A. Garc, J. Junquera, P. Ordej, et al., The SIESTA method for ab initio order- N materials, J. Phys.: Condens Matter. 14 (2002) 2745–2779, http://dx.doi.org/10.1088/0953-8984/14/11/302.
[45] I. Deretzis, A. La Magna, Role of contact bonding on electronic transport in metal-carbon nanotube-metal systems, Nanotechnology 17 (2006) 5063–5072, http://dx.doi.org/10.1088/0957-4484/17/20/005.
[46] S. Sanvito, C.J. Lambert, J.H. Jefferson, A.M. Bratkovsky, General Green's-function formalism for transport calculations with spd Hamiltonians and giant magnetoresistance in Co- and Ni-based magnetic multilayers, Phys. Rev. B 59 (1999) 11936–11948, http://dx.doi.org/10.1103/PhysRevB.59.11936.
[47] C. Cao, A.F. Kemper, L. Agapito, J.-W. Zhang, Y. He, A. Rinzler, et al., Nonequilibrium Green's function study of Pd4-cluster-functionalized carbon nanotubes as hydrogen sensors, Phys. Rev. B 79 (2009) 075127, http://dx.doi.org/10.1103/PhysRevB.79.075127.
[48] C. Toher, S. Sanvito, Effects of self-interaction corrections on the transport properties of phenyl-based molecular junctions, Phys. Rev. B 77 (2008) 155402, http://dx.doi.org/10.1103/PhysRevB.77.155402.
[49] J. Junquera, O. Paz, D. Sanchez-Portal, E. Artacho, Numerical atomic orbitals for linear-scaling calculations, Phys. Rev. B. 64 (2001) 235111, http://dx.doi.org/10.1103/PhysRevB.64.235111.
[50] D.M. Ceperley, B.J. Alder, Ground state of the electron gas by a stochastic model, Phys. Rev. Lett. 45 (1980) 566–569, http://dx.doi.org/10.1103/PhysRevLett.45.566.
[51] J. Tersoff, Schottky barrier heights and the continuum of gap states, Phys. Rev. Lett. 52 (1984) 465–468, http://dx.doi.org/10.1103/PhysRevLett.52.465.
[52] K. Odbadrakh, Theoretical Investigations for Molecular Electronic Devices: Metal/semiconductor Interfaces, Capacitance of Atomic Scale Wires, and Organics on Diamond Surfaces, Ph.D Thesis, North Carolina State University, 2007.
[53] G.T. Feliciano, C. Sanz-Navarro, M.D. Coutinho-Neto, P. Ordejón, R.H. Scheicher, A.R. Rocha, Capacitive DNA detection driven by electronic charge fluctuations in a graphene nanopore, Phys. Rev. Appl. 3 (2015) 034003, http://dx.doi.org/10.1103/PhysRevApplied.3.034003.
[54] I. Rungger, X. Chen, U. Schwingenschlögl, S. Sanvito, Finite-bias electronic transport of molecules in a water solution, Phys. Rev. B 81 (2010) 235407, http://dx.doi.org/10.1103/PhysRevB.81.235407.

Biographies

Sheida Bagherzadeh-Nobari received the B.S. and M.S. degrees in Condensed matter Physics from Islamic Azad University North Tehran Branch, in 2005 and 2008 respectively. She is currently pursuing a Ph.D. degree under the super-vision of Dr. Reza Kalantari-Nejad at Department of physics in Islamic Azad University Science and research Branch. Her research interests include investigation of electrical properties of nano materials as biosensors.

Reza Kalantarinejad graduated at BSc and MSc level in mechanical engineering from Amirkabir University of Tehnology, Tehran, Iran. He conducted his PhD dissertation designing a Nanobiosensor using modern quantum transport approaches. He has several patents and journal papers in the field of nanotechnology and biotech in particular. He is two-time winner of Kharazmi award and has written over 7 books and 20 papers in the field of Nanobiotechnology and Converging Technolgies i.e. NBIC (nano, bio, info and cogno techs). He is an entrepreneur in the field of converging technologies and is the founder of SHEZAN and HAMGARA companies, in which he along with his team have successfully developed relevant technological solutions.

Seyed Mohammad Elahi joined the faculty of Science and Research branch of the Islamic Azad University in 1993. Since that time he has devoted his time and efforts to teaching undergraduate and graduate courses, supervising graduate students, and pursuing research in different interesting fields. As a professor of physics he is conducting research projects in the areas of electrical and optical properties of semiconductor and nano materials, biosensors and gas sensors.

Stefano Sanvito completed his undergraduate studies in Milan (Italy), before moving to the University of Lancaster (UK), where he obtained a PhD in Theoretical Physics. In 2002 he joined the School of Physics, Trinity College Dublin as a contract lecturer, after having spent two successful years as post-doctoral fellow at the University of California Santa Barbara (USA). In 2006 he became Associate Professor in Physics and in 2009 CRANN Deputy Director. At Trinity College Dublin he created the Computational Spintronics Group, a large and dynamical theoretical/computational research group that investigates elementary properties of materials and of nanodevices using computer simulations. He is the author of over hundred and fifty publications including pioneering works on molecular spin-valves and on the ferromagnetism of diluted magnetic semiconductors. Prof Sanvito is a Fellow of Trinity College Dublin and Deputy Director of CRANN.